AGU PUBLICATIONS

JGR

Journal of Geophysical Research: Atmospheres

RESEARCH ARTICLE
10.1002/2016JD025210

Key Points:
- High-resolution simulations with a coupled urban-atmospheric model in China's most rapidly urbanizing regions
- Impacts of urban extent and urban form on climate for regions located in different climate zones at multiple spatiotemporal scales
- Reduced magnitude but increased spatial extent of warming from north to south China

Correspondence to:
D. Yu,
dyyucas@163.com

Citation:
Cao, Q., D. Yu, M. Georgescu, and J. Wu (2016), Impacts of urbanization on summer climate in China: An assessment with coupled land-atmospheric modeling, *J. Geophys. Res. Atmos.*, *121*, doi:10.1002/2016JD025210.

Received 11 APR 2016
Accepted 30 AUG 2016
Accepted article online 3 SEP 2016

Impacts of urbanization on summer climate in China: An assessment with coupled land-atmospheric modeling

Qian Cao[1], Deyong Yu[1], Matei Georgescu[2], and Jianguo Wu[1,3]

[1]Center for Human-Environment System Sustainability, State Key Laboratory of Earth Surface Processes and Resource Ecology, Beijing Normal University, Beijing, China, [2]School of Geographical Sciences and Urban Planning, Arizona State University, Tempe, Arizona, USA, [3]School of Life Sciences and School of Sustainability, Arizona State University, Tempe, Arizona, USA

Abstract China has experienced unprecedented urbanization since the 1980s, resulting in substantial climatic effects from local cities to broad regions. Using the Weather Research and Forecasting model dynamically coupled to an urban canopy model, we quantified the summertime climate effects of urban expansion in China's most rapidly urbanizing regions: Beijing-Tianjin-Hebei (BTH), Yangtze River Delta (YRD), and Pearl River Delta (PRD). High-resolution landscape data of each urban agglomeration for 1988, 2000, and 2010 were used for simulations. Our results indicated summertime urban warming of 0.85°C for BTH, 0.78°C for YRD, and 0.57°C for PRD, which was substantially greater than previous estimates. Peak summer warming for BTH, YRD, and PRD was 1.5°C, 1°C, and 0.8°C, respectively. In contrast, the loss of moisture was greatest in PRD, with maximum reduction in 2 m water vapor mixing ratio close to 1 g/kg, followed by YRD and BTH with local peak humidity deficits reaching 0.8 g/kg and 0.6 g/kg, respectively. Our results were in better agreement with observations than prior studies because of the usage of high-resolution landscape data and the inclusion of key land-atmospheric interactions. Our study also demonstrated that the warming impacts of polycentric urban forms were less intense but more extensive in space, whereas large concentrated urban aggregations produced much stronger but localized warming effects. These findings provide critical knowledge that improves our understanding of urban-atmospheric interactions, with important implications for urban landscape management and planning to alleviate the negative impacts of urban heat islands.

1. Introduction

Urbanization is an extreme case of human modification of the Earth's terrestrial surface and has been recognized to be a highly significant driver of climate change at local and regional scales [*Bornstein*, 1968; *Oke*, 1973; *Portman*, 1993; *Wu*, 2014]. The most recognized manifestation of urbanization-induced climate change is the urban heat island, which has been calculated by observation minus reanalysis [*Kalnay and Cai*, 2003] and modeling/stations-based methods [*Brazel et al*., 2007; *Myint et al*., 2013; *Georgescu et al*., 2014, 2015]. Apart from excessive anthropogenic heating in urban environments [*Feng et al*., 2012, 2013; *Salamanca et al*., 2014; *Sailor et al*., 2015], land surface modification, including high heat-storage capacity, increased impervious surfaces, and decreased vegetation cover of urban environments, alters the surface energy budget with consequences for near-surface warming and alterations to the structure of atmospheric boundary layer [*Georgescu et al*., 2009; *Wang et al*., 2015; *Benson-Lira et al*., 2016]. Therefore, land surface forcing should be considered to accurately assess environmental impacts due to urban expansion, particularly for nations experiencing rapid urbanization [*Creutzig*, 2015; *Georgescu et al*., 2015].

China has witnessed unprecedented socioeconomic development during the previous three decades [*Wu et al*., 2014; *Ma et al*., 2016]. The nation's urbanization rate has risen from 17.9% in 1978 to 54.8% in 2014, and it is expected that 77.5% of its population will be dwelling in cities by 2050 [*Chen et al*., 2013; *Bai et al*., 2014; *Wu et al*., 2014]. Along with the increased urbanization rate (i.e., the proportion of population dwelling in cities) is a rapid expansion of built environments. Based on observations and examination of reanalysis products, statistical studies have indicated an urban expansion-induced warming of 0.05°C per decade in southeast China during 1979–1998 [*Zhou et al*., 2004], 0.11°C per decade in north China during 1961–2000 [*Ren et al*., 2008], and a warming of 0.1°C per decade was observed across east China for the period of 1951–2004 [*Jones et al*., 2008]. Undoubtedly, prior work has highlighted the significance of urbanization-related warming and has paved the way for process-based modeling approaches to characterize the spatiotemporal patterns and physical drivers associated with this type of terrestrial modification.

Numerical models have been increasingly used to estimate climate effects of urbanization for major urbanized areas across China, including the cities of Beijing, Nanjing, Hangzhou, and Wuhan [*Miao et al*., 2009; *Yang et al*., 2012; *Ke et al*., 2013; *Chen et al*., 2014]; the regions of Beijing-Tianjin-Hebei [*Wang et al*., 2013], Yangtze River Delta [*Zhang et al*., 2010; *Liao et al*., 2014], and Pearl River Delta [*Lin et al*., 2009; *Wang et al*., 2014]; and China as a whole [*Feng et al*., 2012, 2013; *Wang et al*., 2012; *Chen and Frauenfeld*, 2015]. The modeling work for these studies was generally focused on capturing urbanization-induced effects (i.e., separate from global warming) by investigating the interactions between the urban canopy and overlying atmosphere. However, prior studies were conducted by incorporating two distinct land use and land cover patterns into climate models, namely, preurban and posturban landscapes, while the landscape complexity of urbanization in between such endpoints (i.e., transition periods that characterize urbanization trends) has been largely omitted. *Lin et al*. [2016] examined the role of urban growth, and its effect on regional climate, by incorporating multiple historical urban snapshots into a stand-alone land surface model, and found urban expansion enhanced regional warming by 0.11, 0.11, and 0.05°C/30 yr in summer for Beijing-Tianjin-Hebei, Yangtze River Delta, and Pearl River Delta, respectively. Although a step forward, the lack of two-way land-atmospheric coupling with coarse spatial resolution (i.e., $0.2° \times 0.2°$) may have resulted in substantial underestimate of the warming effects.

The late 1980s witnessed the revival of urban economy in China, although the phase of the most rapid development became apparent only since 2000 [*Chen et al*., 2013; *Wu et al*., 2014]. In this study, we selected three time snapshots corresponding to 1988, 2000, and 2010 in the nation's urbanization evolution and conducted a suite of high-resolution simulations, via utility of a coupled urban-atmospheric model, to assess climate effects of urban expansion in the three largest urbanizing regions of China: Beijing-Tianjin-Hebei, Yangtze River Delta, and Pearl River Delta (Figure 1). The specific research objectives were (1) to quantify the magnitude of urban expansion during the previous three decades for the three regions; (2) to examine impacts of urban extent and urban form on summer climate of the three regions, with a particular focus on near-surface temperature and humidity; and (3) to comparatively assess how climate effects of urban expansion varied among the three regions located in different climate zones.

2. Study Areas

The Beijing-Tianjin-Hebei (BTH), Yangtze River Delta (YRD), and Pearl River Delta (PRD) metropolitan areas are the most urbanized and industrialized regions of China. They cover only 3.7% of the nation's territory but support 18.2% of its population while contributing 36.8% of its gross domestic product (http://www.stats.gov.cn/). Although the three regions are all located along coastal areas, climate regimes vary notably among them. YRD and PRD are strongly influenced by the East Asian Monsoon with warm and wet summers. The mean summertime temperature for YRD (ranging between 27 and 28°C) is less than that for PRD (30–31°C). By contrast, BTH lies in marginal areas of the monsoonal footprint and thus experiences much drier summer seasons. Although the summer-averaged temperature ranges between 25 and 26°C for BTH, its mean diurnal temperature range of nearly 10°C exceeds that of the other two urban agglomerations by 2–3°C (http://www.cma.gov.cn/).

3. Materials and Methods

3.1. Modeling System and Configuration

Simulations were performed by using the Weather Research and Forecasting (WRF) modeling system with the advanced dynamical solver version 3.6 [*Skamarock et al*., 2008]. Compared with stand-alone land surface models (which are one-way vertical single column models of water and energy fluxes), the WRF model enables two-way coupling between the land surface and the atmosphere, the grid cells of which can interact horizontally via advection, turbulent transport, and diffusion.

The WRF model was configured for high-resolution simulations with one-way triply nested model domains having grid spacing of 27 km, 9 km, and 3 km in both horizontal directions (Figure 1). The coarsest domain, D01, covered almost the entirety of China and extended to the East and South China Sea in order to capture the influence of the East Asian Monsoon on the climate of the three regions, with a total area of 3500 km × 3000 km. The intermediate domain, D02, covered eastern China and enclosed an area of

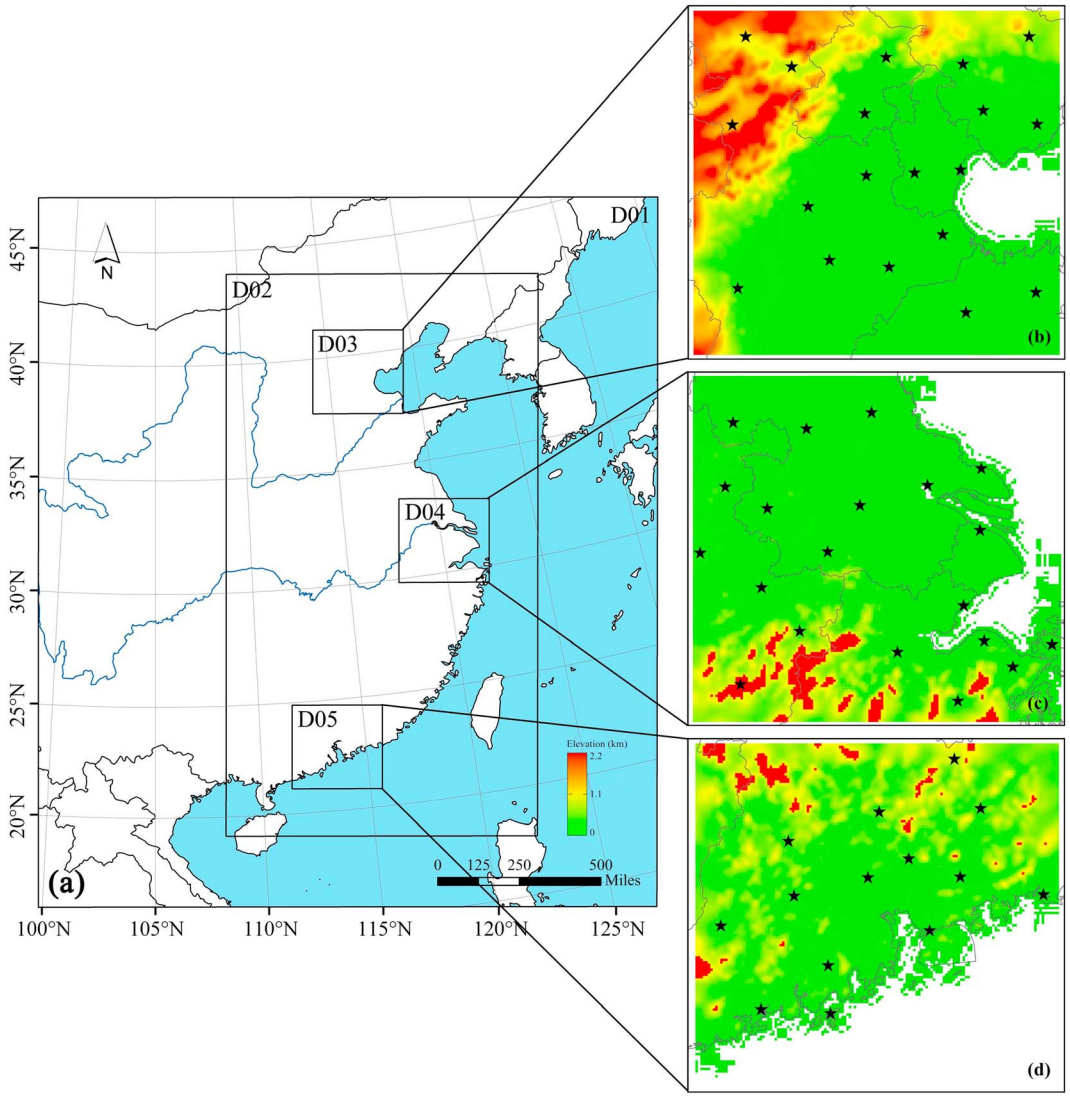

Figure 1. Illustration of the three nested model domains used in the (a) WRF simulations and the monitoring stations in (b) D03, (c) D04, and (d) D05. Domains D03, D04, and D05 locate the three largest urban agglomerations in China: Beijing-Tianjin-Hebei, Yangtze River Delta, and Pearl River Delta. The stations used in the model evaluation are denoted as black stars.

2700 km × 1500 km. The innermost domains, D03, D04, and D05, were centered on the three urban agglomerations and enveloped an area of 444 km × 417 km, respectively. A Lambert conformal conic projection was used for the model's horizontal coordinate, and the model's vertical coordinate employed 30 terrain-following eta levels from the surface to 50 hPa.

The main physical parameterizations used for all simulations are presented in Table 1. In order to represent urban land surface processes (e.g., energy and momentum exchange between urban environments and the atmosphere), the Noah land surface model [*Chen and Dudhia*, 2001] coupled with a single-layer urban canopy model [*Kusaka et al*., 2001; *Kusaka and Kimura*, 2004] was employed. In addition, we used high-intensity residential class (90% constructed material versus 10% pervious surface) to characterize the urbanized areas in BTH, YRD, and PRD, for the following reasons. First, the high-intensity subcategory is predominant in all three urban agglomerations (Figure 2). Second, urban fraction of most urbanized areas in the three regions was up to 90%, or more [e.g., *Liao et al*., 2014]. Indeed, WRF's urban canopy parameters of the high-intensity class, which were presented in *Wang et al*. [2012], were likely to underestimate what they should be in China.

Table 1. Main Physical Parameterizations Used for All Simulations

Model Version:	Version 3.6.1
Horizontal grid (innermost):	Δx and $\Delta y = 3$ km
Number of points (innermost):	148 (x direction), 139 (y direction)
Vertical levels:	30 levels
Time step (innermost):	15 s
Radiation scheme:	RRTM[a] (longwave), RRTMG[b] (shortwave)
Land surface model:	Noah
Urban representation:	Single-layer urban canopy model
Cumulus scheme:	K-F[c] (turned on only for outer two grids)
Microphysics scheme:	WSM-3[d]
PBL scheme:	YSU[e]
Surface layer:	Eta similarity
Initial and lateral boundary conditions:	NCEP FNL/RTG_SST

[a]RRTM, the rapid radiative transfer model.
[b]RRTMG, a new version of RRTM.
[c]K-F, the new Kain-Fritsch cumulus convective scheme.
[d]WSM-3, the WRF single-moment 3 class microphysics scheme.
[e]YSU, the Yonsei University planetary boundary layer (PBL) scheme.

Initial and lateral boundary conditions for large-scale atmospheric fields were provided by the National Centers for Environmental Prediction (NCEP) Global Final Analysis (FNL), with a horizontal resolution of 1°×1° and time interval of 6 h (http://rda.ucar.edu/). It should be noted that the innermost domains are all near the sea, which means that the land-sea interaction will have nonnegligible influence upon urban expansion-induced climate change. However, the WRF model does not predict sea surface temperature (SST), an important parameter that can modify air masses within a short distance from the shore. Therefore, we actively updated SSTs during the simulations by incorporating data from the NCEP's real-time and global SST analysis archives (RTG_SST; ftp://polar.ncep.noaa.gov/) into the WRF model. The data were produced with a daily interval and 0.5° grid spacing in both horizontal directions. In an attempt to have SSTs updated with a 6 h frequency, the daily data were interpolated to a time interval of 6 h prior to the execution of WRF.

3.2. Land Use and Land Cover Data

We obtained land use and land cover data from the Data Sharing Infrastructure of Earth System Science (http://www.geodata.cn/), constructed by the Chinese Academy of Sciences. The data were produced with a spatial resolution of 1 km × 1 km based on Landsat TM remotely sensed imagery so as to monitor nationwide land use and land cover change. In an attempt to assimilate the high-resolution data into climate models and improve the accuracy of model simulations, the data were classified according to the International Geosphere-Biosphere Programme land use classification scheme, with an overall accuracy of 83.14% [*Liu et al*., 2014]. In this study, land use and land cover corresponding to 1988, 2000, and 2010 were utilized as surface boundary conditions (Figure 3). Overall, urban extent of the three regions indicated steady growth during 1988–2000, followed by a phase of rapid expansion during 2000–2010, particularly for BTH and YRD

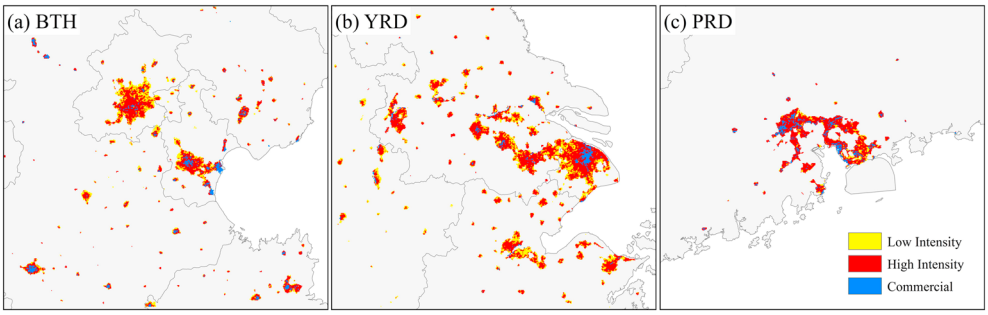

Figure 2. Urban land use classification for (a) BTH, (b) YRD, and (c) PRD in 2009. Impervious surface fraction no more than 50% was mapped to low intensity, 50–80% to high intensity, and more than 80% to characterize commercial [*Homer et al*., 2007]. The impervious surface data were obtained from *Ma et al*. [2014].

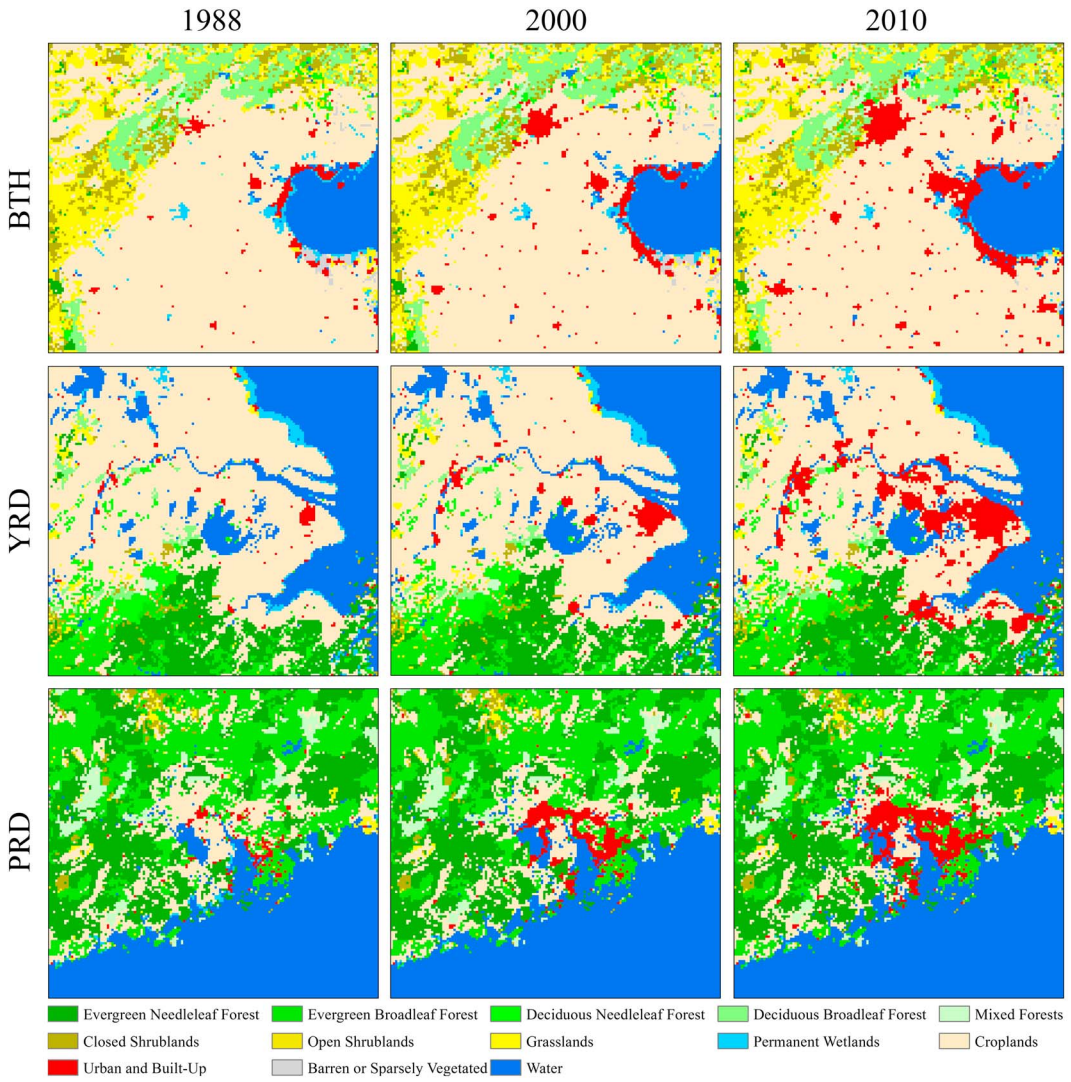

Figure 3. Land use and land cover conditions corresponding to 1988, 2000, and 2010 in Beijing-Tianjin-Hebei, Yangtze River Delta, and Pearl River Delta.

(Figure 4). Urban expansion largely occurred at the expense of the cropland (Figure 4). Our newly developed land use and land cover data were only used for the innermost domains, and for the outer two domains, the default land surface conditions provided by the WRF modeling system were employed.

3.3. Numerical Simulation Design

We designed three numerical experiments by using surface boundary conditions relative to 1988 (Urb1988), 2000 (Urb2000), and 2010 (Urb2010), respectively. Prior to execution of high-resolution simulations, we selected three normal summers as driving forces (we defined summer as June, July, and August). Our selection of representative summers was based on examination of the observed record in eastern China for the period of 2000–2010 [*Sun et al.*, 2014]. The summers of 2001, 2003, and 2005 were chosen for the following reasons. First, summertime temperature anomalies of the 3 years were relatively low compared to those of the three hottest summers during the previous decade (i.e., 2000, 2007, and 2010), at 0.6°C, 0.3°C, and 0.5°C above the 1955–1984 30 year average [*Sun et al.*, 2014]. These summers were therefore characterized as representative of mean summertime conditions. Second, to account for the potential variability among this subset of summers, continuous June-July-August seasons were not simulated to better distinguish the signal of urban expansion-induced forcing [*Georgescu*, 2015]. Simulations were then initialized on 25 May at 00:00 UTC of the corresponding year and continued through 31 August at 18:00 UTC of the equivalent year for each

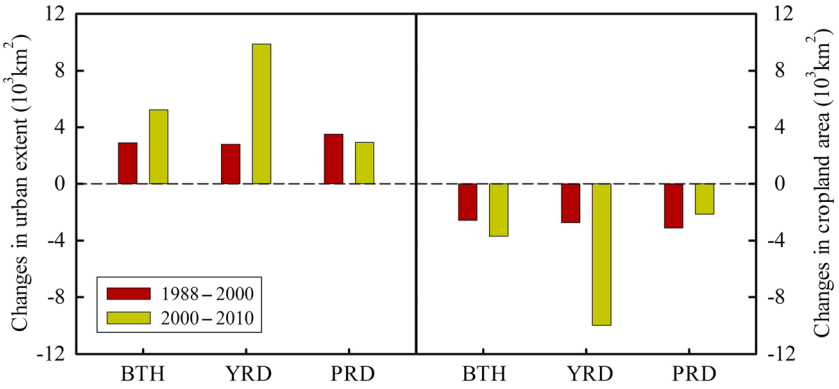

Figure 4. Changes in urban extent and cropland area in Beijing-Tianjin-Hebei, Yangtze River Delta, and Pearl River Delta during the periods of 1988–2000 (dark red) and 2000–2010 (dark yellow).

experiment. The initial week of all simulations was regarded as spin-up and thus excluded from the following analyses. In total, nine simulations were performed in our study (Table 2).

3.4. Model Evaluation Data

To evaluate the time-varying and spatially explicit model performance, both station-based and gridded observations were used in our study. The station-based observations were from "SURF_CLI_CHN_MUL_DAY," a data set provided by the China Meteorological Data Network (http://data.cma.gov.cn/). The data set contained daily meteorological information for observing stations across mainland China. Overall, there were 19, 20, and 14 stations within D03, D04, and D05, respectively. For model evaluation, observed daily maximum, minimum, and mean temperatures during the summers of 2001, 2003, and 2005 were utilized. Because of the relatively coarse grid spacing (i.e., 3 km) used for our simulations relative to location-based observations covering an area of 1 m^2, observations were further averaged across all stations within each domain (Figure 1) and compared to the corresponding average of simulated grid cells, which were nearest to the station locations. This approach is commonly used within the mesoscale modeling community given the resolution gap between observational stations and numerical modeling grid cells [e.g., *Georgescu et al*., 2011, 2015; *Salamanca et al*., 2014; *Benson-Lira et al*., 2016].

In addition, gridded observations provided by the National Climate Center of China Meteorological Administration were utilized to examine WRF's capability of representing spatially explicit thermal characteristics. The gridded data were produced based on interpolation of 751 observing stations in mainland China, for the purpose of climate model validation [*Xu et al*., 2009]. It provides monthly mean air temperatures for the period of 1961–2012 with a spatial resolution of 0.25° × 0.25°. To facilitate model examination, mean 2 m air temperatures simulated by the WRF model across all three summers were compared to the corresponding mean summer temperatures derived from the gridded observations.

Table 2. Description of All Simulations Performed[a]

Simulations	Spin-Up Period	Analysis Time
Urb1988	25–31 May 2001	1 Jun to 31 Aug 2001
	25–31 May 2003	1 Jun to 31 Aug 2003
	25–31 May 2005	1 Jun to 31 Aug 2005
Urb2000	25–31 May 2001	1 Jun to 31 Aug 2001
	25–31 May 2003	1 Jun to 31 Aug 2003
	25–31 May 2005	1 Jun to 31 Aug 2005
Urb2010	25–31 May 2001	1 Jun to 31 Aug 2001
	25–31 May 2003	1 Jun to 31 Aug 2003
	25–31 May 2005	1 Jun to 31 Aug 2005

[a]Urb1988: simulations utilizing urban extent for 1988. Urb2000: simulations utilizing urban extent for 2000. Urb2010: simulations utilizing urban extent for 2010. All simulations were initialized on 25 May of the equivalent year and terminated on 31 Aug of the corresponding year. The initial week was regarded as spin-up and thus excluded from the following analyses.

Table 3. Model Evaluation Against Station-Based Observations for Beijing-Tianjin-Hebei (BTH), Yangtze River Delta (YRD), and Pearl River Delta (PRD) Across all Three Summers (2001, 2003, and 2005)[a]

		2001		2003		2005	
		OBS	WRF	OBS	WRF	OBS	WRF
BTH	Average	25.8	27.3 (+1.5)	24.7	25.7 (+1.0)	25.7	27.0 (+1.3)
	Maximum	31.2	32.8 (+1.6)	29.9	30.7 (+0.8)	31.1	32.0 (+0.9)
	Minimum	21.2	21.2 (+0.0)	20.2	20.1 (−0.1)	21.1	21.3 (+0.2)
YRD	Average	26.2	27.4 (+1.2)	26.8	28.1 (+1.3)	27.1	28.1 (+1.0)
	Maximum	30.0	31.4 (+1.4)	31.1	32.4 (+1.3)	31.3	32.4 (+1.1)
	Minimum	23.2	23.4 (+0.2)	23.5	23.4 (−0.1)	23.8	23.7 (−0.1)
PRD	Average	27.8	28.7 (+0.9)	28.6	29.1 (+0.5)	28.1	28.9 (+0.8)
	Maximum	31.9	32.3 (+0.4)	32.9	32.8 (−0.1)	32.2	32.4 (+0.2)
	Minimum	25.1	25.2 (+0.1)	25.4	25.5 (+0.1)	25.4	25.4 (+0.0)

[a]The observations were averaged across all stations within each domain and compared to the corresponding average of simulated grid cells, which were nearest to the station locations. Model bias is presented in parentheses. Units are in degree Celsius.

4. Results

4.1. WRF Model Evaluation

To evaluate the performance of the WRF model, we compared the simulated 2 m air temperatures from Urb2000 with both the station-based and gridded observations. The simulated nighttime minimum temperatures agreed well with the observations for all three summers in the three regions, with absolute errors no more than 0.2°C (Table 3). WRF-simulated daily mean and daytime maximum temperatures for PRD indicated an absolute error less than 1°C for all three summers, while those for the other two regions demonstrated a positive bias less than 1.6°C. The simulated daily mean temperatures also agreed reasonably well with the observations for each of the urban agglomerations during all three summers (Figure 5). When the observations exhibited a sharp increase in temperatures, the model followed accordingly; conversely, when the observations indicated a steep decrease in temperatures, the model reproduced such change appropriately.

Comparison of simulated summertime temperatures averaged across all three summers with the corresponding gridded observations demonstrated WRF's capability to reproduce the spatial variability of temperatures with reasonable fidelity (Figure 6). For example, the simulation successfully captured high temperatures of the three domains in North China Plain, the lower reaches of Yangtze River Plain, and Pearl River Delta Plain, as well as low temperatures in the mountains and hills located in northwest BTH, southernmost YRD, and north PRD. However, the locations of the highest temperatures differed between the simulation and the observation in certain places, particularly for YRD and PRD. This discrepancy was ascribed to the limitations of gridded observations because the interpolation of observational stations failed to account for the impacts of SSTs on near-surface temperatures [*Xu et al*., 2009].

The simulation results presented here indicate a model bias that is at least as good as what has been shown in prior studies [e.g., *Miao et al*., 2009; *Wang et al*., 2012; *Wang et al*., 2014]. The relatively better model performance may be attributable to the usage of real-time SSTs, as PRD and YRD are strongly influenced by the East Asian Monsoon during summer. In addition, the parameterization schemes used in our simulations may also play a critical role [*Yang et al*., 2015]. The systemic discrepancies between the simulation and the observation were likely caused by errors in initial and lateral boundary conditions or intrinsic limitations of WRF. However, because the WRF model compared at least as favorably as recent similar investigations in respect to both time-varying and spatially varying observations, we deemed it a suitably useful tool for the examination of impacts associated with historical urban expansion.

4.2. Climatic Effects of Historical Urban Expansion

We calculated the ensemble differences in 2 m air temperatures between different numerical experiments to estimate impacts of urban expansion on summertime climate of the three urban agglomerations. Results indicated that the magnitude and spatial pattern of near-surface warming varied considerably among the three regions (Figure 7). Urbanization had the strongest local warming effects in BTH using 2010 urban extent, with maximum warming ranging from 1.2°C to 1.5°C for the majority of urban areas. Somewhat

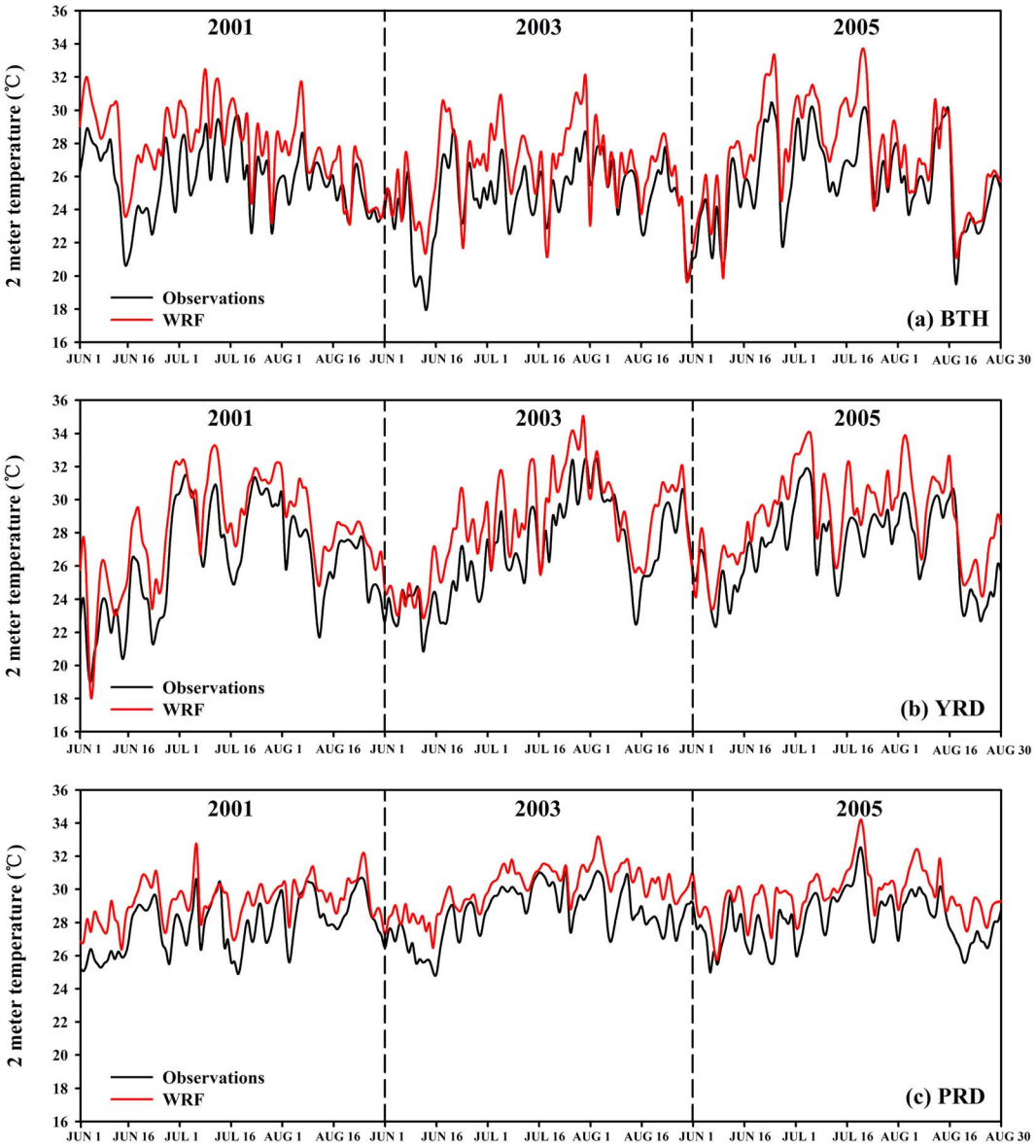

Figure 5. Observed (black curve) and WRF-simulated (red curve) daily mean time series of 2 m air temperatures (°C) during all three summers (2001, 2003, and 2005) in (a) Beijing-Tianjin-Hebei, (b) Yangtze River Delta, and (c) Pearl River Delta.

reduced warming, on the order of 1°C, was found in YRD, while broad warming of less than 0.8°C appeared in PRD. Overall, increases in 2 m air temperatures by 0.85°C, 0.78°C, and 0.57°C, averaged only for urban pixels of 2010, were estimated in BTH, YRD, and PRD, respectively. It is notable that near-surface warming was generally restricted to no more than 0.6°C in coastal locations for all urbanized regions.

The spatial extent of urban expansion-induced warming extended far beyond the built environments of YRD, where regionalized warming effects were discernible at earlier stages of urbanization (i.e., by 2000) and were greatly reinforced after an additional 10 years of urban sprawl (i.e., by 2010). This did not seem to be the case for BTH where near-surface warming was somewhat confined to its built-up areas. The sphere of influence can be described by an *effect index* that is defined $EI(x) = A_{change}(x)/A_{urban}$ as, where x denotes any meteorological parameter, $A_{change}(x)$denotes the area where x changed, and A_{urban} denotes the urban area. An EI equal to 1 indicates only that urban locations are affected, <1 signifies only parts of the urban locations are affected, and >1 represents the effects extend beyond the built environments. By 2000, EIs of 1.4, 4.1, and 2.5 were estimated for BTH, YRD, and PRD, while by 2010, the EI values were increased to 2.7, 5.0, and 3.6, respectively.

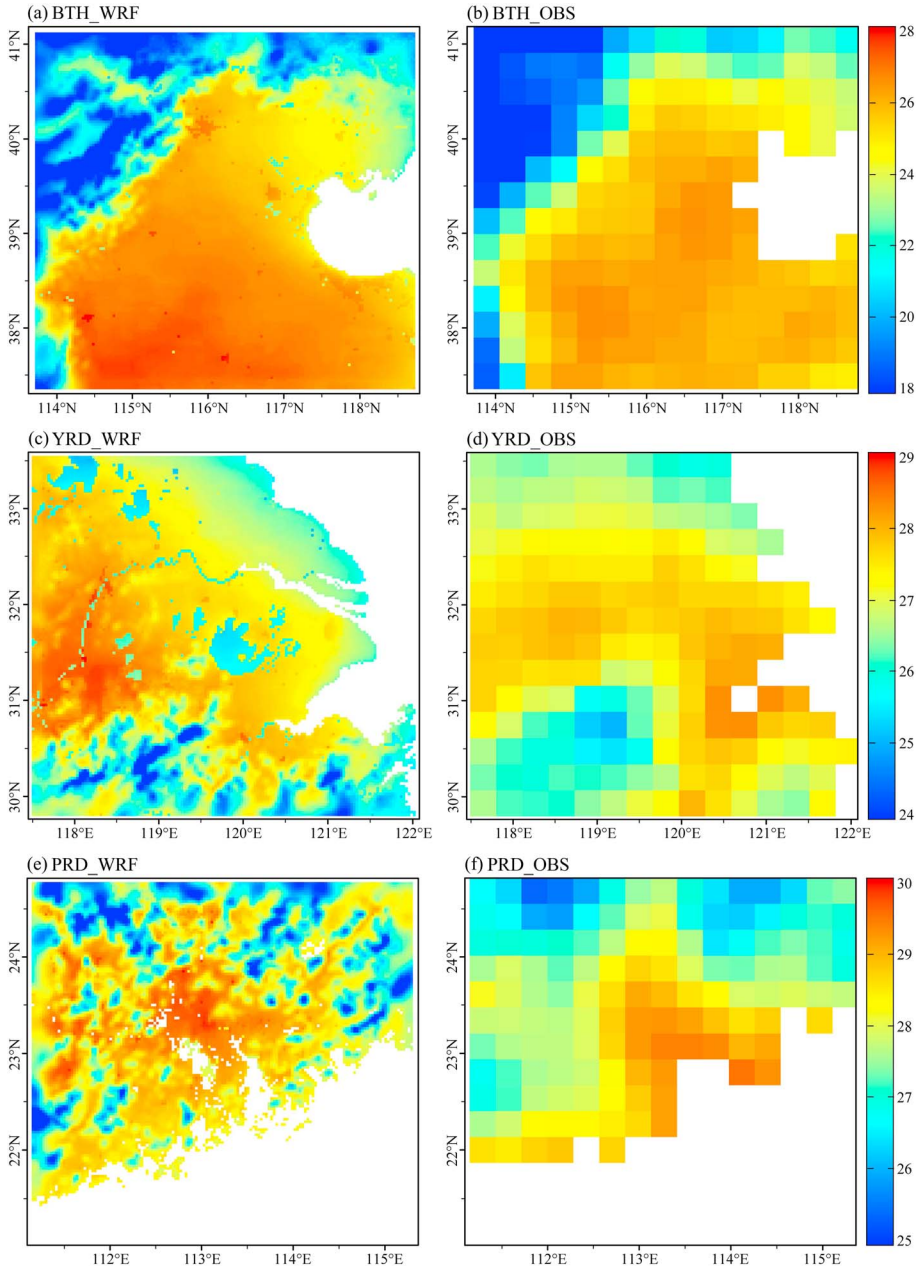

Figure 6. Spatial pattern of WRF-simulated and observed mean summertime 2 m air temperatures (°C), averaged across all three summers (2001, 2003, and 2005), in (a and b) Beijing-Tianjin-Hebei, (c and d) Yangtze River Delta, and (e and f) Pearl River Delta.

Differences in maximum (T_{max}), minimum (T_{min}), and diurnal temperature range (DTR; $T_{max} - T_{min}$), averaged only for urban grid cells of 2010, illustrated the effects of urban expansion on the reduction of the diurnal temperature range by increasing minimum temperatures (Figure 8). The region displaying the largest increase in T_{min} and thus decrease in DTR was BTH, followed by YRD and then PRD. On the contrary, PRD produced the maximum increase in T_{max} during roughly three decades of urban expansion, with the full range of simulated variability ranging between 0.2 and 0.5°C by 2010. Slightly reduced daytime warming was simulated for YRD, while no significant changes in T_{max} were estimated for BTH. By 2010, the net effects of changes in T_{min} and T_{max} reduced the DTR by 0.8–1.8°C for BTH and 0.9–1.3°C for YRD. Increases in both T_{max} and T_{min} in PRD resulted in relatively reduced changes in DTR from 2000 to 2010 (between 0.2 and 1°C).

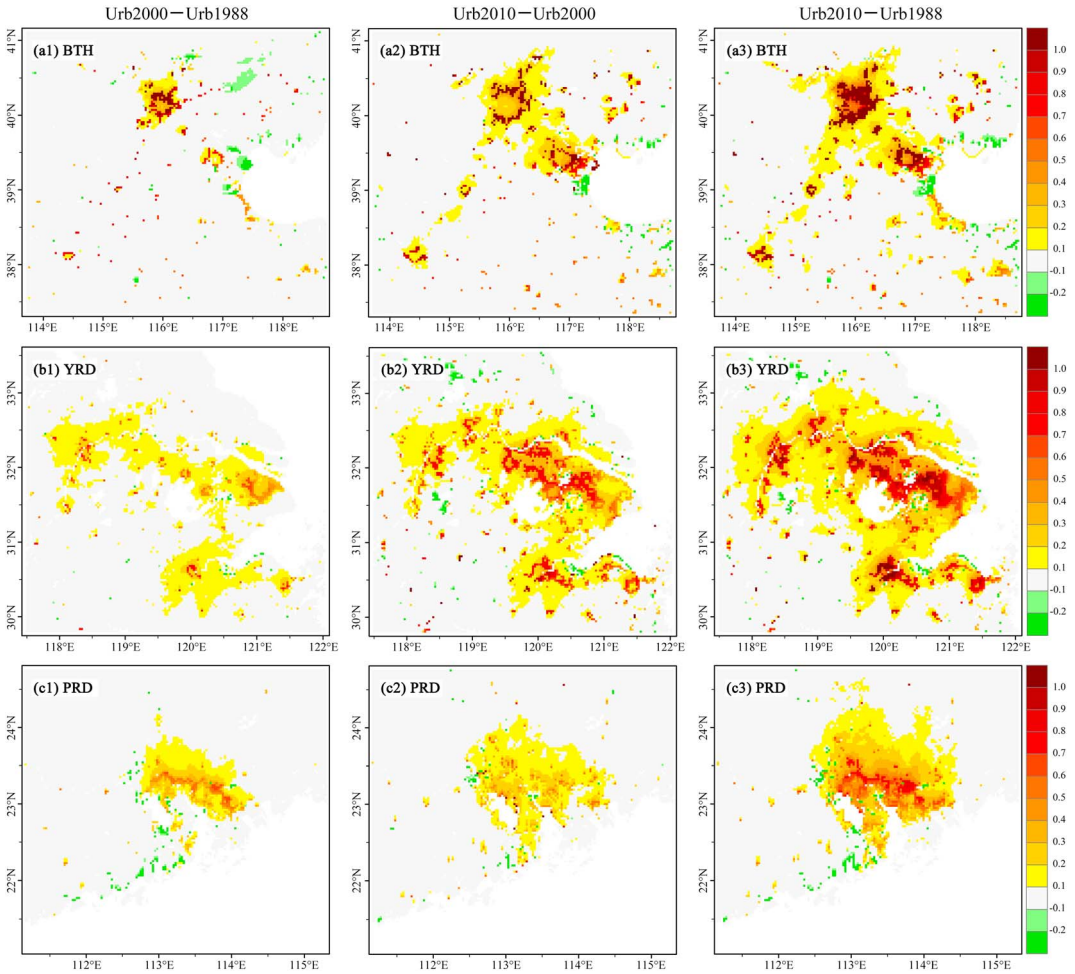

Figure 7. Spatial pattern of changes in WRF-simulated mean summertime 2 m air temperatures (°C) between different numerical experiments (i.e., Urb2000–Urb1988, left column; Urb2010–Urb2000, middle column; and Urb2010–Urb1988, right column) in (a1, a2, and a3) Beijing-Tianjin-Hebei, (b1, b2, and b3) Yangtze River Delta, and (c1, c2, and c3) Pearl River Delta.

The degree to which simulated differences in T_{min} and T_{max} agreed with observations can provide additional confidence in WRF's capability to reproduce the changing summer climate of the three urban agglomerations. As expected, observed time series of mean summertime T_{max} and T_{min} for the period of 1980–2010 at urban stations of the three regions exhibited enhanced nighttime relative to daytime effects (Figure 9). In addition, no significant linear trend of T_{max} ($p > 0.05$) was observed in BTH, while increased T_{max} was evident ($p < 0.01$) in both YRD and PRD. The observations agreed with our simulations, which also indicated increased T_{max} in YRD and PRD, but no such trend in BTH (see Figure 8). The demonstrated level of skill for the simulations presented here, grounded on accurate depiction of thermal impacts associated with historically observed patterns of urbanization in China, can pave the way for future simulations to characterize the climate effects of projected urban expansion-induced climate change.

As illustrated by Figure 10, time series of daily mean 2 m air temperature (T_{avg}) differences, once again averaged only at urban locales of 2010, for the duration of summer indicated that urban expansion markedly increased T_{avg} of BTH during August and T_{avg} of YRD during both July and August. However, the warming effects tended to be reduced from June to August in PRD, and the increased T_{avg} was of similar magnitude, on the order of 0.25°C (i.e., Urb2010–Urb2000), throughout the summer season. Overall, the degree and daily variability of changes in T_{avg} were strongest in BTH, followed by YRD, while those in PRD were of smaller magnitude and less variability. The simulation results agreed well with observations indicating that the trend of warming was highest and most significant ($p < 0.01$) in August, for BTH, during 1980–2010 (Figure 11).

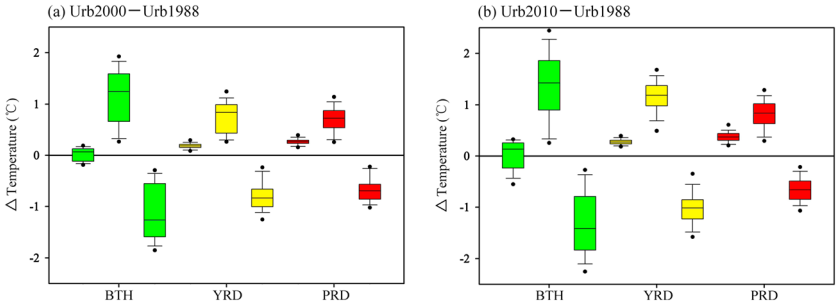

Figure 8. The box and whisker plots of WRF-simulated differences in summertime 2 m maximum (left of the color trio), minimum (center of the color trio), and diurnal temperature range (right of the color trio) in Beijing-Tianjin-Hebei (green), Yangtze River Delta (yellow), and Pearl River Delta (red) between Urb2000 and Urb1988 (a; Urb2000–Urb1988), as compared to those between Urb2010 and Urb1988 (b; Urb2010-Urb1988). Calculations were performed only for urban grid cells of 2010. The unit is degree Celsius.

Likewise, trends of warming observed at YRD urban stations were greater in July and August. By contrast, changing summertime air temperatures over PRD were insignificant (in June and August) or of smaller magnitude (in July). Once again, maximum trends of warming, for the duration of summer, still occurred in YRD.

We further examined alterations to surface energy budget between Urb2010 and Urb1988 (Figure 12) to improve understanding of the physical drivers of near-surface temperature changes. Results indicated that net radiation decreased slightly in all three regions throughout the day, and it was mainly because of higher skin temperatures and thus larger upward longwave radiation at built-up surfaces. Expansion of built environments further led to increased sensible heat but decreased latent heat during the day, with the latter showing much greater daytime than nighttime effects. However, ground heat flux was reduced during the daytime (i.e., downwelling solar energy was stored within urban infrastructure) but raised during the nighttime (i.e., release of the energy from urban environments). In accordance with reduced net radiation, changes

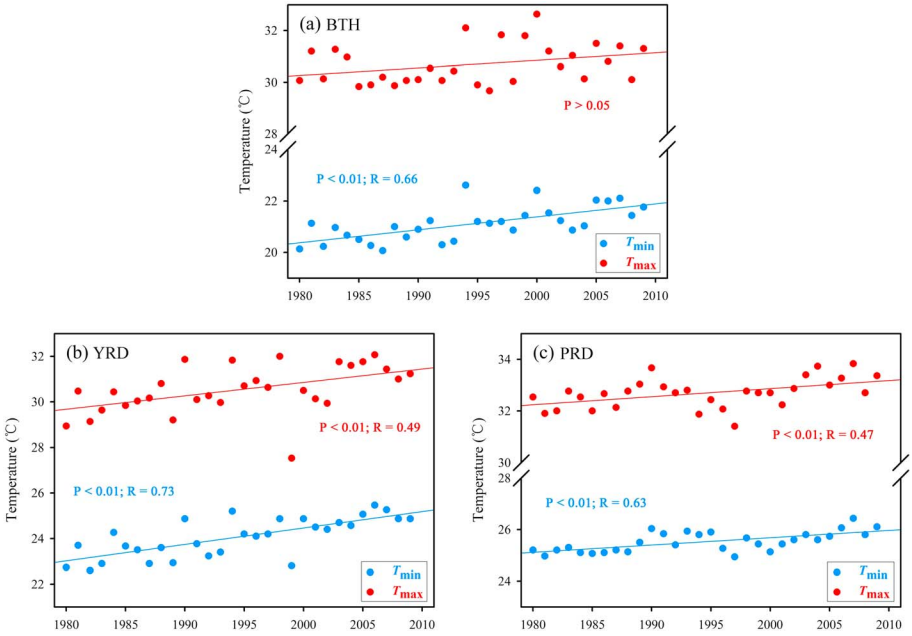

Figure 9. Observed time series of mean summertime maximum and minimum temperatures (°C) at urban stations of (a) Beijing-Tianjin-Hebei, (b) Yangtze River Delta, and (c) Pearl River Delta for the period of 1980–2010. The straight lines represent trend of the time series using a linear least squares fitting technique. The following eight stations were used: (1) Beijing (39.79°N, 116.46°E), (2) Shijiazhuang (38.03°N, 114.41°E), (3) Tianjin (39.08°N, 117.06°E), (4) Shanghai (31.40°N, 121.45°E), (5) Nanjing (32.00°N, 118.80°E), (6) Hangzhou (30.23°N, 120.16°E), (7) Shenzhen (22.53°N, 114.00°E), and (8) Guangzhou (23.16°N, 113.33°E).

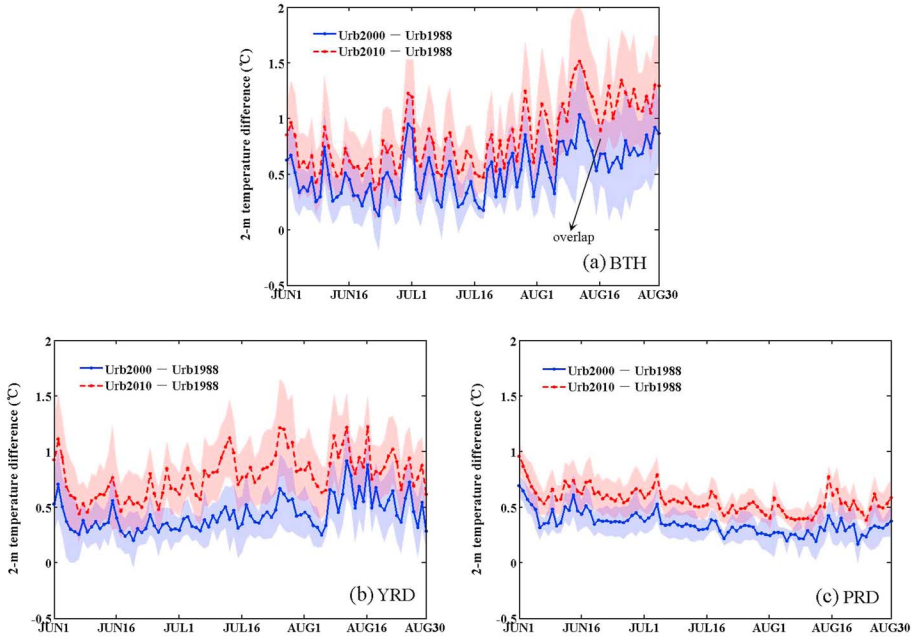

Figure 10. WRF-simulated time series of daily mean 2 m air temperature differences (°C) between Urb2000 and Urb1988 (Urb2000-Urb1988; blue solid line), as compared to those between Urb2010 and Urb1988 (Urb2010-Urb1988; red dashed line) in (a) Beijing-Tianjin-Hebei, (b) Yangtze River Delta, and (c) Pearl River Delta. Calculations were performed only for urban grid cells of 2010. The shaded areas represent 1 standard deviation above and below the mean.

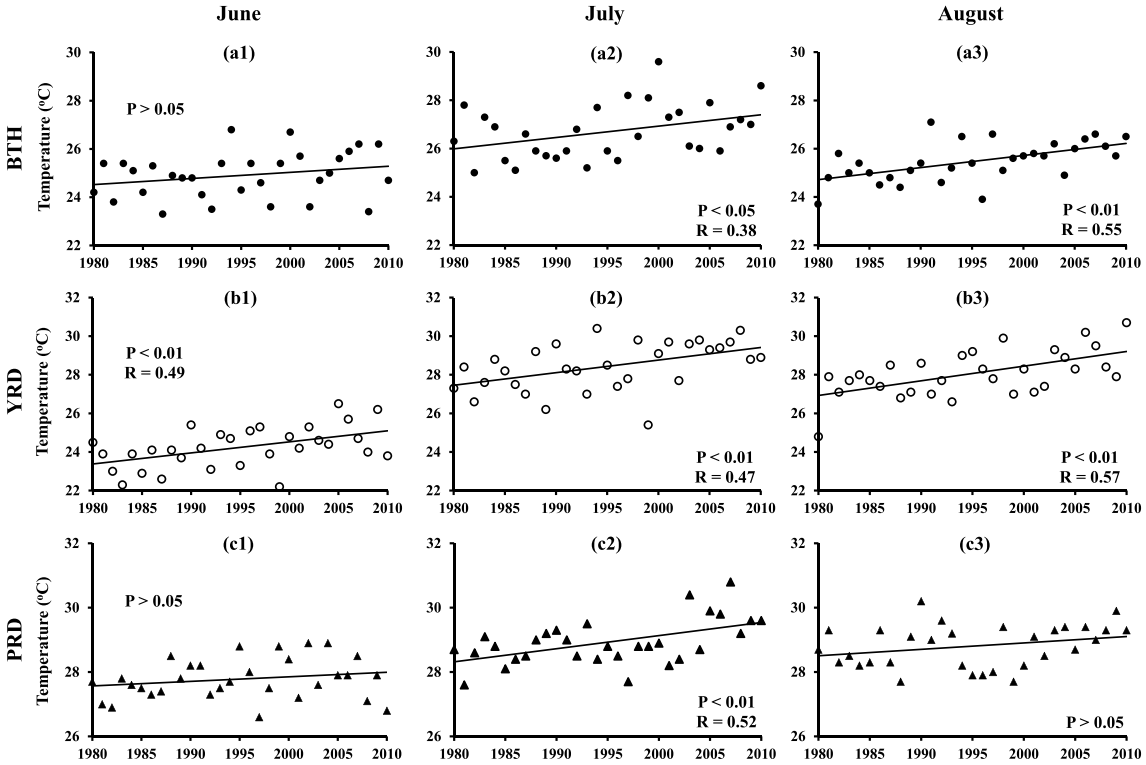

Figure 11. Observed time series of mean air temperatures (°C) during June, July, and August, respectively, for the period of 1980–2010 at urban stations of (a1, a2, and a3) Beijing-Tianjin-Hebei, (b1, b2, and b3) Yangtze River Delta, and (c1, c2, and c3) Pearl River Delta. The stations used are the same as Figure 9.

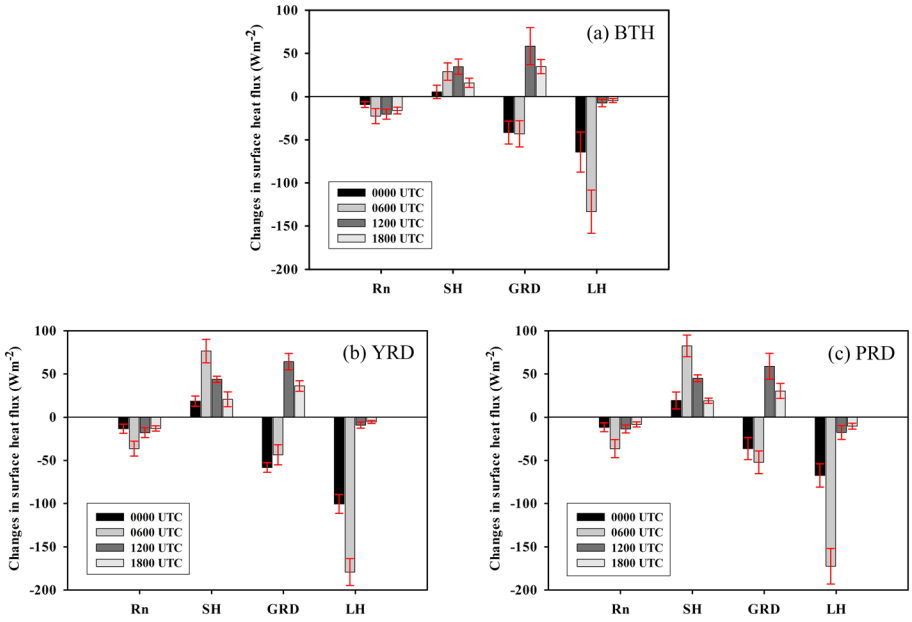

Figure 12. Differences in summertime mean net radiation flux (R_n; Wm^{-2}), sensible heat flux (SH; Wm^{-2}), ground heat flux (GRD; Wm^{-2}), and latent heat flux (LH; Wm^{-2}) at 00:00, 06:00, 12:00, and 18:00 UTC (i.e., 08:00, 14:00, 20:00, and 02:00 local standard time) between Urb2010 and Urb1988 (Urb2010–Urb1988) in (a) Beijing-Tianjin-Hebei, (b) Yangtze River Delta, and (c) Pearl River Delta. The negative GRD indicates the energy storage. The error bars represent 1 standard deviation above and below the mean. Calculations were performed only for urban grid cells of 2010.

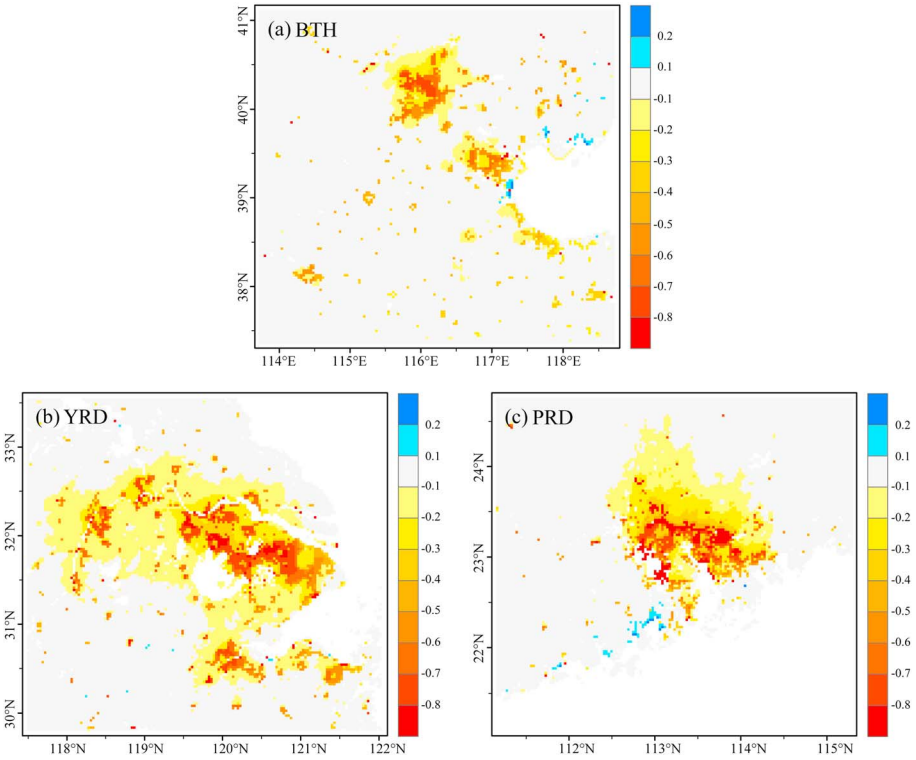

Figure 13. Spatial pattern of ensemble differences in WRF-simulated mean summertime 2 m water vapor mixing ratio ($g\,kg^{-1}$) between Urb2010 and Urb1988 (Urb2010–Urb1988) in (a) Beijing-Tianjin-Hebei, (b) Yangtze River Delta, and (c) Pearl River Delta.

in ground heat flux were of lesser magnitude than the combined changes in sensible and latent heat flux by day, but of greater magnitude at night. This occurred because evapotranspiration was decreased substantially in the daytime due to less moisture availability in urban areas, while a great deal of energy was lost from built structures during nighttime hours.

Simulated changes in 2 m water vapor mixing ratio between Urb2010 and Urb1988 (Figure 13) indicated that the greatest low-level atmospheric moisture decrease was simulated for PRD, on the order of 1 g/kg. Slightly reduced levels of moisture, up to 0.8 g/kg, was found in the majority of YRD urban locations, while BTH produced the minimum reductions in near-surface moisture, with 0.6 g/kg on average in its urban grid cells. This occurred because YRD and PRD are strongly influenced by the East Asian Monsoon, which brings the two regions abundant moisture in summer. Instead, BTH is located in north China with much drier summer seasons. Therefore, urban expansion imposed greater impacts on near-surface moisture over YRD and PRD than it did over BTH. Notable exceptions were still coastal locations, where a reduced degree of humidity deficit was simulated compared to nearby inland cities. Once again, the widespread drying effects extended far beyond the urban areas of YRD, with the effect index, EI, close to 4, followed by PRD (EI = 3.2), whereas such effects were still restricted to the built environments of BTH, with EI equivalent to 1.6.

5. Discussion

5.1. Climatic Effects of Historical Urban Expansion

Climatic effects of historical urbanization were examined for the three largest urban agglomerations of China through assessment of changes in near-surface climate metrics (i.e., temperature and humidity). The magnitude of urban expansion-induced warming revealed by our simulations was 0.85°C, 0.78°C, and 0.57°C for the urban locations of BTH, YRD, and PRD, by 2010, with local peak warming reaching 1.5°C, 1°C, and 0.8°C, respectively. Our results were comparable with a prior study reporting urbanization-induced increases in summer temperatures by 1.42°C, 1.74°C, and 1.27°C (nonurban landscape versus 2009 urban landscape) in the urbanized areas of the three regions, respectively [*Wang et al*., 2012]. However, our study disagreed with that of *Lin et al*. [2016], whose simulations led to regionally averaged summer warming of 0.11°C/30 yr, 0.11°C/30 yr, and 0.05°C/30 yr for BTH, YRD, and PRD, with local maximum warming of merely 0.2°C for all three regions. *Lin et al*. [2016] significantly underestimated the observations indicating urban expansion-induced warming by at least 0.3°C/30 yr in major urbanized regions of China [*Jones et al*., 2008; *Ren et al*., 2008] and the simulated results from our study.

The discrepancies between our study and that of *Lin et al*. [2016] may be ascribed to the following reasons. First, lack of two-way coupling between the land surface and the atmosphere in a stand-alone land surface model utilized by *Lin et al*. [2016] was a likely contributing factor in the underestimate of simulated warming, while our study used a coupled urban-atmospheric model that also enables the interaction between its simulated grid cells. Second, the landscape patterns employed by our study were derived from high-resolution remotely sensed imagery of the corresponding years. Conversely, the urban fraction within a grid box of $0.2° \times 0.2°$ used by *Lin et al*. [2016] can neither describe the specific urban extent nor the urban form, thus limiting their capability to accurately quantify how the evolving urban landscape patterns affect regional climate.

It should be noted that the observations indicated that urban expansion imposed the strongest warming in YRD. This occurred because the observed record integrates modifications in land surface conditions, anthropogenic heat release, and emissions of long-lived greenhouse gases, while we did not account for the latter two contributing factors in our work: we focused on the impacts of urban land expansion on regional climate. According to *Feng et al*. [2012, 2013], mean annual anthropogenic heat release in major metropolises of YRD was larger than that in BTH and YRD. However, we did not intend to compare the absolute value but rather the trend of simulated temperature changes with the observations. Future regional climate analysis should incorporate the decadal evolution of anthropogenic heat release and the evolving nature of greenhouse gas emissions.

It is clear that urban environments with distinctive thermal properties will absorb and store energy during the daytime and release the energy during the nighttime, thus giving rise to considerable nighttime warming [*Grimmond and Oke*, 1999]. Changes in daytime temperatures, however, were largely dependent on climate

regime [*Zhao et al*., 2014]. According to prior studies focusing on urbanization in arid regions [*Georgescu et al*., 2011, 2015], urban expansion can reduce daytime temperatures because of increased energy storage by built structures (i.e., decreased sensible heat flux during the daytime due to enhanced energy storage relative to the prior land use). This did not seem to be the case for YRD and PRD, whose climate conditions were much cooler and wetter, thus restricting the heating capacity of constructed materials compared to arid regions. Consequently, portions of the absorbed insolation by day will be partitioned into sensible heat that warms near-surface temperatures. Prior work conducted on the corresponding regions was consistent with our study in regard to the increased maximum temperatures due to urbanization [e.g., *Zhang et al*., 2010; *Wang et al*., 2014].

Although it was the partitioning of available energy into sensible heat and latent heat that largely determined the warming effects in the built environments of the three regions [*Wang et al*., 2012; *Chen and Frauenfeld*, 2015; *Lin et al*., 2016], the amount of incoming solar radiation also made a difference. For example, PRD is located in subtropical areas with more solar energy being absorbed by day, hence the highest degree of daytime warming. However, no significant changes in daytime temperatures occurred in BTH, since the sparsely distributed inland cities in the south lowered temperatures by day. With regard to the magnitude of nighttime warming, differences in background thermal advection were of importance. For example, YRD and PRD are strongly influenced by land-sea interactions that result in horizontal thermal advection over the two regions. By contrast, BTH is dominated by vertical thermal advection as it is located in a basin surrounded by high mountains. This, in turn, affected the spatial extent of near-surface warming. Findings of *Chen and Frauenfeld* [2015] were in accord with our study indicating increased daytime warming but decreased nighttime warming from north to south China.

Apart from background climate, urban landscape morphology also plays a nonnegligible role in shaping the spatial variability of urbanization-induced warming [*Yang et al*., 2016]. As illustrated, BTH and YRD experienced dissimilar urban expansion patterns during the previous three decades, with the former experiencing concentrated sprawl and the latter polycentric sprawl. As a result, built environment-induced warming and drying effects were greater locally in BTH, while notable regionalized effects were found in YRD at earlier stages of the urbanizing process. Near-surface temperature and humidity in northern parts of PRD, though far from the urban locales, were also affected by urbanization due to zonal arrangement of its constructed materials that hindered the transport of cool and moist air from the nearby sea. Hence, there is a trade-off between urban form and urban extent in an attempt to achieve "resource-efficient and environment-friendly" urban landscapes in China.

5.2. Implications for Future Research

Our study highlights that urban landscape management and planning is an effective way to alleviate climate warming due to urbanization. However, it is still not clear how the arrangement of urban landscapes (i.e., the total amount and morphology) will simultaneously boost economic growth while minimizing its deleterious impacts on climate. As the space left for urbanization in the three regions is becoming increasingly restricted, a shift in urban expansion pattern from sprawl to infill is likely to be prevalent for future urban development in China [*Normile*, 2016]. Therefore, a critical issue should stimulate our attention as to how the intensity of constructed structures (e.g., proportion of impervious surfaces, height of buildings, and density of roads) will affect climate if urban extent remains the same over time [*Yang et al*., 2016]. In addition, while our study focused on mean summertime conditions so as to better distinguish the signal of urban expansion-induced forcing, future work should also address extreme summers and heat events. For instance, synergistic effects between urban heat islands and heat waves may result in compounding health-related consequences that are further exacerbated under conditions of blackouts or general infrastructure failure [*Li and Bou-Zeid*, 2013]. Indeed, a nascent area of research lies at the intersection of urban infrastructure and socioeconomic resilience [*Hondula et al*., 2015]. Accounting for the dynamic interplay between social and physical systems, thus characterizing feedback among them, will facilitate development of sustainable urban environments.

6. Conclusions

This study established the first comprehensive assessment of how, and to what extent, urban extent, urban form, and climate regime affected the summer climate of the three largest urban agglomerations in China, namely, Beijing-Tianjin-Hebei, Yangtze River Delta, and Pearl River Delta, using an atmospheric model

dynamically coupled to an urban canopy model. The magnitude of warming for the urbanized areas of the three regions was 0.85°C, 0.78°C, and 0.57°C, with local peak warming up to 1.5°C, 1°C, and 0.8°C, respectively. Compared with prior work targeted on the same regions [e.g., *Lin et al*., 2016], our simulations, with the incorporation of real-time SSTs, the usage of historical high-resolution land use/land cover patterns, and the employment of coupled urban-atmospheric model substantially improved the performance of WRF and the accuracy of simulated impacts in regard to both the magnitude and spatial pattern. Our findings underscore the significance of interactions between urban landscape and overlying atmosphere and have practical implications for mitigating urban heat islands and climate change via land system planning.

Acknowledgments
The initial and lateral boundary conditions for WRF simulations were provided by the NCEP FNL data set (http://rda.ucar.edu/) and the NCEP SST archives (ftp://polar.ncep.noaa.gov/). Land use and land cover data were provide by the Data Sharing Infrastructure of Earth System Science (http://www.geodata.cn/). We used station-based observations obtained from the China Meteorological Data Network (http://data.cma.gov.cn/) and gridded observations produced by *Xu et al*. [2009] from the National Climate Center for model evaluation. This study was supported by the National Basic Research Program of China grant 2014CB954301, Fund for Creative Research Groups of National Natural Science Foundation of China grant 41321001, the 111 Project "Hazard and Risk Science Base at Beijing Normal University" grant B08008, and the Project of State Key Laboratory of Earth Surface Processes and Resources Ecology. M.G. was supported by NSF grants EAR-1204774, DMS-1419593, and SES-1520803, NSF Sustainable Research Network grant CBET-1444758, and by USDA NIFA grant 2015-67003-23508.

References

Bai, X., P. Shi, and Y. Liu (2014), Society: Realizing China's urban dream, *Nature*, *509*, 158–160.
Benson-Lira, V., M. Georgescu, S. Kaplan, and E. R. Vivoni (2016), Loss of a lake system in a megacity: The impact of urban expansion on seasonal meteorology in Mexico City, *J. Geophys. Res. Atmos.*, *121*, 3079–3099, doi:10.1002/2015JD024102.
Bornstein, R. D. (1968), Observations of the urban heat island effect in New York City, *J. Appl. Meteorol.*, *7*, 575–582.
Brazel, A., P. Gober, S. Lee, S. Grossman-Clarke, J. Zehnder, B. Hedquist, and E. Comparri (2007), Determinants of changes in the regional urban heat island in metropolitan Phoenix (Arizona, USA) between 1990 and 2004, *Clim. Res.*, *33*, 171–182.
Chen, F., and J. Dudhia (2001), Coupling an advanced land surface-hydrology model with the Penn State-NCAR MM5 modeling system. Part I: Model implementation and sensitivity, *Mon. Weather Rev.*, *129*, 569–585.
Chen, F., X. Yang, and W. Zhu (2014), WRF simulations of urban heat island under hot-weather synoptic conditions: The case study of Hangzhou City, China, *Atmos. Res.*, *138*, 364–377.
Chen, L., and O. W. Frauenfeld (2015), Impacts of urbanization on future climate in China, *Clim. Dynam.*, doi:10.1007/s00382-015-2840-6.
Chen, M., W. Liu, and X. Tao (2013), Evolution and assessment on China's urbanization 1960–2010: Under-urbanization or over-urbanization?, *Habitat Int.*, *38*, 25–33.
Creutzig, F. (2015), Towards typologies of urban climate and global environmental change, *Environ. Res. Lett.*, *10*, 101001.
Feng, J., Y. Wang, Z. Ma, and Y. Liu (2012), Simulating the regional impacts of urbanization and anthropogenic heat release on climate across China, *J. Clim.*, *25*, 7187–7203.
Feng, J., Y. Wang, and Z. Ma (2013), Long-term simulation of large-scale urbanization effect on the East Asian monsoon, *Clim. Change*, *129*, 511–523.
Georgescu, M., G. Miguez-Macho, L. T. Steyaert, and C. P. Weaver (2009), Climatic effects of 30 years of landscape change over the Greater Phoenix, Arizona, region: 1. Surface energy budget changes, *J. Geophys. Res.*, *114*, D05110, doi:10.1029/2008JD010745.
Georgescu, M., M. Moustaoui, A. Mahalov, and J. Dudhia (2011), An alternative explanation of the semiarid urban area "oasis effect", *J. Geophys. Res.*, *116*, D24113, doi:10.1029/2011JD016720.
Georgescu, M., P. E. Morefield, B. G. Bierwagen, and C. P. Weaver (2014), Urban adaptation can roll back warming of emerging megapolitan regions, *Proc. Natl. Acad. Sci. U.S.A.*, *111*, 2909–2914.
Georgescu, M. (2015), Challenges associated with adaptation to future urban expansion, *J. Clim.*, *28*, 2544–2563.
Georgescu, M., W. Chow, Z. Wang, A. Brazel, B. Trapido-Lurie, M. Roth, and V. Benson-Lira (2015), Prioritizing urban sustainability solutions: Coordinated approaches must incorporate scale-dependent built environment induced effects, *Environ. Res. Lett.*, *10*, 061001.
Grimmond, C. S. B., and T. R. Oke (1999), Heat storage in urban areas: Local-scale observations and evaluation of a simple model, *J. Appl. Meteorol.*, *38*, 922–940.
Homer, C., J. Dewitz, J. Fry, M. Coan, N. Hossain, C. Larson, N. Herold, A. McKerrow, N. VanDriel, and J. Wickham (2007), Completion of the 2001 national land cover database for the counterminous United States, *Photogramm. Eng. Rem. S.*, *73*, 337–341.
Hondula, D. M., R. C. Balling Jr., J. K. Vanos, and M. Georgescu (2015), Rising temperatures, human health, and the role of adaptation, *Curr. Clim. Change Rep.*, *1*, 144–154.
Jones, P. D., D. H. Liser, and Q. Li (2008), Urbanization effects in large-scale temperature records, with an emphasis on China, *J. Geophys. Res.*, *113*, D16122, doi:10.1029/2008JD009916.
Kalnay, E., and M. Cai (2003), Impact of urbanization and land-use change on climate, *Nature*, *423*, 528–531.
Ke, X., F. Wu, and C. Ma (2013), Scenario analysis on climate change impacts of urban land expansion under different urbanization patterns: A case study of Wuhan metropolitan, *Adv. Meteorol.*, *2013*, 293,636.
Kusaka, H., H. Kondo, Y. Kikegawa, and F. Kimura (2001), A simple single-layer urban canopy model for atmospheric models: Comparison with multi-layer and slab models, *Boundary Layer Meteorol.*, *101*, 329–358.
Kusaka, H., and F. Kimura (2004), Coupling a single-layer urban canopy model with a simple atmospheric model: Impact on urban heat island simulation for an idealized case, *J. Meteorol. Soc. Jpn.*, *82*, 67–80.
Li, D., and E. Bou-Zeid (2013), Synergistic interactions between urban heat islands and heat waves: The impact in cities is larger than the sum of its parts, *J. Appl. Meteorol. Climatol.*, *52*, 2051–2064.
Liao, J., T. Wang, X. Wang, M. Xie, Z. Jiang, X. Huang, and J. Zhu (2014), Impacts of different urban canopy schemes in WRF/Chem on regional climate and air quality in Yangtze River Delta, China, *Atmos. Res.*, *145*, 226–243.
Lin, S., J. Feng, J. Wang, and Y. Hu (2016), Modeling the contribution of long-term urbanization to temperature increase in three extensive urban agglomerations in China, *J. Geophys. Res. Atmos.*, *121*, 1683–1697, doi:10.1002/2015JD024227.
Lin, W., L. Zhang, D. Du, L. Yang, H. Lin, Y. Zhang, and J. Li (2009), Quantification of land use/land cover changes in Pearl River Delta and its impact on regional climate in summer using numerical modeling, *Reg. Environ. Change*, *9*, 75–82.
Liu, J., et al. (2014), Spatiotemporal characteristics, patterns and causes of land use changes in China since the late 1988, *J. Geogr. Sci.*, *69*, 3–14.
Ma, Q., C. He, J. Wu, Z. Liu, Q. Zhang, and Z. Sun (2014), Quantifying spatiotemporal patterns of urban impervious surfaces in China: An improved assessment using nighttime light data, *Landscape Urban Plan.*, *130*, 36–49.
Ma, Q., J. Wu, and C. He (2016), A hierarchical analysis of the relationship between urban impervious surfaces and land surface temperatures: Spatial scale dependence, temporal variations, and bioclimatic modulation, *Landscape Ecol.*, *31*, 1139–1153.
Miao, S., F. Chen, M. A. LeMone, M. Tewari, Q. Li, and Y. Wang (2009), An observational and modeling study of characteristics of urban heat island and boundary layer structures in Beijing, *J. Appl. Meteorol. Climatol.*, *48*, 484–501.

Myint, S. W., E. A. Wentz, A. J. Brazel, and D. A. Quattrochi (2013), The impact of distinct anthropogenic and vegetation features on urban warming, *Landscape Ecol.*, *28*, 959–978.
Normile, D. (2016), China rethinks cities, *Science*, *352*, 916–918.
Oke, T. R. (1973), City size and the urban heat island, *Atmos. Environ.*, *7*, 769–779.
Portman, D. A. (1993), Identifying and correcting urban bias in regional time series: Surface temperature in China's northern plains, *J. Clim.*, *6*, 2298–2308.
Ren, G., Y. Zhou, Z. Chu, J. Zhou, A. Zhang, J. Guo, and X. Liu (2008), Urbanization effects on observed surface air temperature trends in north China, *J. Clim.*, *21*, 1333–1348.
Sailor, D. J., M. Georgescu, J. M. Milne, and M. A. Hart (2015), Development of a national anthropogenic heating database with an extrapolation for international cities, *Atmos. Environ.*, *118*, 7–18.
Salamanca, F., M. Georgescu, A. Mahalov, M. Moustaoui, and M. Wang (2014), Anthropogenic heating of the urban environment due to air conditioning, *J. Geophys. Res. Atmos.*, *119*, 5949–5965, doi:10.1002/2013JD021225.
Skamarock, W. C., J. B. Klemp, J. Dudhia, D. O. Gill, D. M. Barker, W. Wang, and J. G. Powers (2008), A description of the advanced research WRF version 3 (No. NCAR/TN-475 + STR), *NCAR Technical Note*, doi:10.5065/D68S4MVH.
Sun, Y., X. Zhang, F. W. Zwiers, L. Song, H. Wan, T. Hu, H. Yin, and G. Ren (2014), Rapid increase in the risk of extreme summer heat in Eastern China, *Nature Clim. Change*, *4*, 1082–1085.
Wang, J., J. Feng, Z. Yan, Y. Hu, and G. Jia (2012), Nested high-resolution modeling of the impact of urbanization on regional climate in three vast urban agglomerations in China, *J. Geophys. Res.*, *117*, D21103, doi:10.1029/2012JD018226.
Wang, L., Z. Gao, S. Miao, X. Guo, T. Sun, M. Liu, and D. Li (2015), Contrasting characteristics of the surface energy balance between the urban and rural areas of Beijing, *Adv. Atmos. Sci.*, *32*, 505–514.
Wang, M., X. Zhang, and X. Yan (2013), Modeling the climatic effects of urbanization in the Beijing-Tianjin-Hebei metropolitan area, *Theor. Appl. Climatol.*, *113*, 377–385.
Wang, X., J. Liao, J. Zhang, C. Shen, W. Chen, B. Xia, and T. Wang (2014), A numeric study of regional climate change induced by urban expansion in the Pearl River Delta, China, *J. Appl. Meteorol. Climatol.*, *53*, 346–362.
Wu, J. (2014), Urban ecology and sustainability: The state-of-the-science and future directions, *Landscape Urban Plan.*, *125*, 209–221.
Wu, J., W. Xiang, and J. Zhao (2014), Urban ecology in China: Historical developments and future directions, *Landscape Urban Plan.*, *125*, 222–233.
Xu, Y., X. Gao, Y. Shen, C. Xu, Y. Shi, and F. Giorgi (2009), A daily temperature dataset over China and its application in validating a RCM simulation, *Adv. Atmos. Sci.*, *26*, 763–772.
Yang, B., Y. Zhang, and Y. Qian (2012), Simulation of urban climate with high-resolution WRF model: A case study in Nanjing, China, *Asia-Pacific J. Atmos. Sci.*, *48*, 227–241.
Yang, B., Y. Zhang, Y. Qian, A. Huang, and H. Yan (2015), Calibration of a convective parameterization scheme in the WRF model and its impact on the simulation of East Asian summer monsoon precipitation, *Clim. Dynam.*, *44*, 1661–1684.
Yang, L., D. Niyogi, M. Tewari, D. Aliaga, F. Chen, F. Tian, and G. Ni (2016), Contrasting impacts of urban forms on the future thermal environment: Example of Beijing metropolitan area, *Environ. Res. Lett.*, *11*, 034018.
Zhang, N., Z. Gao, X. Wang, and Y. Chen (2010), Modeling the impact of urbanization on the local and regional climate in Yangtze River Delta, China, *Theor. Appl. Climatol.*, *102*, 331–342.
Zhao, L., X. Lee, R. B. Smith, and K. Oleson (2014), Strong contributions of local background climate to urban heat islands, *Nature*, *511*, 216–219.
Zhou, L., R. E. Dickinson, Y. Tian, J. Fang, Q. Li, R. K. Kaufmann, C. J. Tucker, and R. B. Myneni (2004), Evidence for a significant urbanization effect on climate in China, *Proc. Natl. Acad. Sci. U.S.A.*, *101*, 9540–9544.